Fermi National Accelerator Laboratory

FERMILAB-Pub-98/091-E
REVISED
CDF

Observation of $B^+ \to \psi(2S)\ K^+$ and $B^0 \to \psi(2S)\ K^*(892)^0$ Decays and Measurements of B-meson Branching Fractions into J/ψ and $\psi(2S)$ Final States

F. Abe et al.
The CDF Collaboration

Fermi National Accelerator Laboratory
P.O. Box 500, Batavia, Illinois 60510

August 1998

Submitted to *Physical Review D*

Operated by Universities Research Association Inc. under Contract No. DE-AC02-76CH03000 with the United States Department of Energy

Disclaimer

This report was prepared as an account of work sponsored by an agency of the United States Government. Neither the United States Government nor any agency thereof, nor any of their employees, makes any warranty, expressed or implied, or assumes any legal liability or responsibility for the accuracy, completeness, or usefulness of any information, apparatus, product, or process disclosed, or represents that its use would not infringe privately owned rights. Reference herein to any specific commercial product, process, or service by trade name, trademark, manufacturer, or otherwise, does not necessarily constitute or imply its endorsement, recommendation, or favoring by the United States Government or any agency thereof. The views and opinions of authors expressed herein do not necessarily state or reflect those of the United States Government or any agency thereof.

Distribution

Approved for public release; further dissemination unlimited.

FERMILAB-Pub-98/091-E
CDF/PUB/BOTTOM/PUBLIC/4425
Version 3.02

Observation of $B^+ \to \psi(2S)\,K^+$ and $B^0 \to \psi(2S)\,K^*(892)^0$ decays and measurements of B-meson branching fractions into J/ψ and $\psi(2S)$ final states

F. Abe,[17] H. Akimoto,[39] A. Akopian,[31] M. G. Albrow,[7] A. Amadon,[5] S. R. Amendolia,[27] D. Amidei,[20] J. Antos,[33] S. Aota,[37] G. Apollinari,[31] T. Arisawa,[39] T. Asakawa,[37] W. Ashmanskas,[18] M. Atac,[7] P. Azzi-Bacchetta,[25] N. Bacchetta,[25] S. Bagdasarov,[31] M. W. Bailey,[22] P. de Barbaro,[30] A. Barbaro-Galtieri,[18] V. E. Barnes,[29] B. A. Barnett,[15] M. Barone,[9] G. Bauer,[19] T. Baumann,[11] F. Bedeschi,[27] S. Behrends,[3] S. Belforte,[27] G. Bellettini,[27] J. Bellinger,[40] D. Benjamin,[35] J. Bensinger,[3] A. Beretvas,[7] J. P. Berge,[7] J. Berryhill,[5] S. Bertolucci,[9] S. Bettelli,[27] B. Bevensee,[26] A. Bhatti,[31] K. Biery,[7] C. Bigongiari,[27] M. Binkley,[7] D. Bisello,[25] R. E. Blair,[1] C. Blocker,[3] S. Blusk,[30] A. Bodek,[30] W. Bokhari,[26] G. Bolla,[29] Y. Bonushkin,[4] D. Bortoletto,[29] J. Boudreau,[28] L. Breccia,[2] C. Bromberg,[21] N. Bruner,[22] R. Brunetti,[2] E. Buckley-Geer,[7] H. S. Budd,[30] K. Burkett,[20] G. Busetto,[25] A. Byon-Wagner,[7] K. L. Byrum,[1] M. Campbell,[20] A. Caner,[27] W. Carithers,[18] D. Carlsmith,[40] J. Cassada,[30] A. Castro,[25] D. Cauz,[36] A. Cerri,[27] P. S. Chang,[33] P. T. Chang,[33] H. Y. Chao,[33] J. Chapman,[20] M. -T. Cheng,[33] M. Chertok,[34] G. Chiarelli,[27] C. N. Chiou,[33] F. Chlebana,[7] L. Christofek,[13] M. L. Chu,[33] S. Cihangir,[7] A. G. Clark,[10] M. Cobal,[27] E. Cocca,[27] M. Contreras,[5] J. Conway,[32] J. Cooper,[7] M. Cordelli,[9] D. Costanzo,[27] C. Couyoumtzelis,[10] D. Cronin-Hennessy,[6] R. Culbertson,[5] D. Dagenhart,[38] T. Daniels,[19] F. DeJongh,[7] S. Dell'Agnello,[9] M. Dell'Orso,[27] R. Demina,[7] L. Demortier,[31] M. Deninno,[2] P. F. Derwent,[7] T. Devlin,[32] J. R. Dittmann,[6] S. Donati,[27] J. Done,[34] T. Dorigo,[25] N. Eddy,[20] K. Einsweiler,[18] J. E. Elias,[7] R. Ely,[18] E. Engels, Jr.,[28] W. Erdmann,[7] D. Errede,[13] S. Errede,[13] Q. Fan,[30] R. G. Feild,[41] Z. Feng,[15] C. Ferretti,[27] I. Fiori,[2] B. Flaugher,[7] G. W. Foster,[7] M. Franklin,[11] J. Freeman,[7] J. Friedman,[19] Y. Fukui,[17] S. Gadomski,[14] S. Galeotti,[27] M. Gallinaro,[26] O. Ganel,[35] M. Garcia-Sciveres,[18] A. F. Garfinkel,[29] C. Gay,[41] S. Geer,[7] D. W. Gerdes,[15] P. Giannetti,[27] N. Giokaris,[31] P. Giromini,[9] G. Giusti,[27] M. Gold,[22] A. Gordon,[11] A. T. Goshaw,[6] Y. Gotra,[25] K. Goulianos,[31] H. Grassmann,[36] L. Groer,[32] C. Grosso-Pilcher,[5] G. Guillian,[20] J. Guimaraes da Costa,[15] R. S. Guo,[33] C. Haber,[18] E. Hafen,[19] S. R. Hahn,[7] R. Hamilton,[11] T. Handa,[12] R. Handler,[40] F. Happacher,[9] K. Hara,[37] A. D. Hardman,[29] R. M. Harris,[7] F. Hartmann,[16] J. Hauser,[4] E. Hayashi,[37] J. Heinrich,[26] W. Hao,[35] B. Hinrichsen,[14] K. D. Hoffman,[29] M. Hohlmann,[5] C. Holck,[26] R. Hollebeek,[26] L. Holloway,[13] Z. Huang,[20] B. T. Huffman,[28] R. Hughes,[23] J. Huston,[21] J. Huth,[11] H. Ikeda,[37] M. Incagli,[27] J. Incandela,[7] G. Introzzi,[27] J. Iwai,[39] Y. Iwata,[12] E. James,[20] H. Jensen,[7] U. Joshi,[7] E. Kajfasz,[25] H. Kambara,[10] T. Kamon,[34] T. Kaneko,[37] K. Karr,[38] H. Kasha,[41] Y. Kato,[24] T. A. Keaffaber,[29] K. Kelley,[19] R. D. Kennedy,[7] R. Kephart,[7] D. Kestenbaum,[11] D. Khazins,[6] T. Kikuchi,[37] B. J. Kim,[27] H. S. Kim,[14] S. H. Kim,[37] Y. K. Kim,[18] L. Kirsch,[3] S. Klimenko,[8] D. Knoblauch,[16] P. Koehn,[23] A. Köngeter,[16] K. Kondo,[37] J. Konigsberg,[8]

K. Kordas,[14] A. Korytov,[8] E. Kovacs,[1] W. Kowald,[6] J. Kroll,[26] M. Kruse,[30] S. E. Kuhlmann,[1] E. Kuns,[32] K. Kurino,[12] T. Kuwabara,[37] A. T. Laasanen,[29] I. Nakano,[12] S. Lami,[27] S. Lammel,[7] J. I. Lamoureux,[3] M. Lancaster,[18] M. Lanzoni,[27] G. Latino,[27] T. LeCompte,[1] S. Leone,[27] J. D. Lewis,[7] P. Limon,[7] M. Lindgren,[4] T. M. Liss,[13] J. B. Liu,[30] Y. C. Liu,[33] N. Lockyer,[26] O. Long,[26] C. Loomis,[32] M. Loreti,[25] D. Lucchesi,[27] P. Lukens,[7] S. Lusin,[40] J. Lys,[18] K. Maeshima,[7] P. Maksimovic,[19] M. Mangano,[27] M. Mariotti,[25] J. P. Marriner,[7] A. Martin,[41] J. A. J. Matthews,[22] P. Mazzanti,[2] P. McIntyre,[34] P. Melese,[31] M. Menguzzato,[25] A. Menzione,[27] E. Meschi,[27] S. Metzler,[26] C. Miao,[20] T. Miao,[7] G. Michail,[11] R. Miller,[21] H. Minato,[37] S. Miscetti,[9] M. Mishina,[17] S. Miyashita,[37] N. Moggi,[27] E. Moore,[22] Y. Morita,[17] A. Mukherjee,[7] T. Muller,[16] P. Murat,[27] S. Murgia,[21] H. Nakada,[37] I. Nakano,[12] C. Nelson,[7] D. Neuberger,[16] C. Newman-Holmes,[7] C.-Y. P. Ngan,[19] L. Nodulman,[1] A. Nomerotski,[8] S. H. Oh,[6] T. Ohmoto,[12] T. Ohsugi,[12] R. Oishi,[37] M. Okabe,[37] T. Okusawa,[24] J. Olsen,[40] C. Pagliarone,[27] R. Paoletti,[27] V. Papadimitriou,[35] S. P. Pappas,[41] N. Parashar,[27] A. Parri,[9] J. Patrick,[7] G. Pauletta,[36] M. Paulini,[18] A. Perazzo,[27] L. Pescara,[25] M. D. Peters,[18] T. J. Phillips,[6] G. Piacentino,[27] M. Pillai,[30] K. T. Pitts,[7] R. Plunkett,[7] A. Pompos,[29] L. Pondrom,[40] J. Proudfoot,[1] F. Ptohos,[11] G. Punzi,[27] K. Ragan,[14] D. Reher,[18] M. Reischl,[16] A. Ribon,[25] F. Rimondi,[2] L. Ristori,[27] W. J. Robertson,[6] T. Rodrigo,[27] S. Rolli,[38] L. Rosenson,[19] R. Roser,[13] T. Saab,[14] W. K. Sakumoto,[30] D. Saltzberg,[4] A. Sansoni,[9] L. Santi,[36] H. Sato,[37] P. Schlabach,[7] E. E. Schmidt,[7] M. P. Schmidt,[41] A. Scott,[4] A. Scribano,[27] S. Segler,[7] S. Seidel,[22] Y. Seiya,[37] F. Semeria,[2] T. Shah,[19] M. D. Shapiro,[18] N. M. Shaw,[29] P. F. Shepard,[28] T. Shibayama,[37] M. Shimojima,[37] M. Shochet,[5] J. Siegrist,[18] A. Sill,[35] P. Sinervo,[14] P. Singh,[13] K. Sliwa,[38] C. Smith,[15] F. D. Snider,[15] J. Spalding,[7] T. Speer,[10] P. Sphicas,[19] F. Spinella,[27] M. Spiropulu,[11] L. Spiegel,[7] L. Stanco,[25] J. Steele,[40] A. Stefanini,[27] R. Ströhmer,[7] J. Strologas,[13] F. Strumia,[10] D. Stuart,[7] K. Sumorok,[19] J. Suzuki,[37] T. Suzuki,[37] T. Takahashi,[24] T. Takano,[24] R. Takashima,[12] K. Takikawa,[37] M. Tanaka,[37] B. Tannenbaum,[22] F. Tartarelli,[27] W. Taylor,[14] M. Tecchio,[20] P. K. Teng,[33] Y. Teramoto,[24] K. Terashi,[37] S. Tether,[19] D. Theriot,[7] T. L. Thomas,[22] R. Thurman-Keup,[1] M. Timko,[38] P. Tipton,[30] A. Titov,[31] S. Tkaczyk,[7] D. Toback,[5] K. Tollefson,[19] A. Tollestrup,[7] H. Toyoda,[24] W. Trischuk,[14] J. F. de Troconiz,[11] S. Truitt,[20] J. Tseng,[19] N. Turini,[27] T. Uchida,[37] F. Ukegawa,[26] J. Valls,[32] S. C. van den Brink,[28] S. Vejcik, III,[20] G. Velev,[27] R. Vidal,[7] R. Vilar,[7] D. Vucinic,[19] R. G. Wagner,[1] R. L. Wagner,[7] J. Wahl,[5] N. B. Wallace,[27] A. M. Walsh,[32] C. Wang,[6] C. H. Wang,[33] M. J. Wang,[33] A. Warburton,[14] T. Watanabe,[37] T. Watts,[32] R. Webb,[34] C. Wei,[6] H. Wenzel,[16] W. C. Wester, III,[7] A. B. Wicklund,[1] E. Wicklund,[7] R. Wilkinson,[26] H. H. Williams,[26] P. Wilson,[5] B. L. Winer,[23] D. Winn,[20] D. Wolinski,[20] J. Wolinski,[21] S. Worm,[22] X. Wu,[10] J. Wyss,[27] A. Yagil,[7] W. Yao,[18] K. Yasuoka,[37] G. P. Yeh,[7] P. Yeh,[33] J. Yoh,[7] C. Yosef,[21] T. Yoshida,[24] I. Yu,[7] A. Zanetti,[36] F. Zetti,[27] and S. Zucchelli[2]

(CDF Collaboration)

[1] *Argonne National Laboratory, Argonne, Illinois 60439*
[2] *Istituto Nazionale di Fisica Nucleare, University of Bologna, I-40127 Bologna, Italy*
[3] *Brandeis University, Waltham, Massachusetts 02254*
[4] *University of California at Los Angeles, Los Angeles, California 90024*
[5] *University of Chicago, Chicago, Illinois 60637*
[6] *Duke University, Durham, North Carolina 27708*
[7] *Fermi National Accelerator Laboratory, Batavia, Illinois 60510*
[8] *University of Florida, Gainesville, Florida 32611*
[9] *Laboratori Nazionali di Frascati, Istituto Nazionale di Fisica Nucleare, I-00044 Frascati, Italy*
[10] *University of Geneva, CH-1211 Geneva 4, Switzerland*
[11] *Harvard University, Cambridge, Massachusetts 02138*
[12] *Hiroshima University, Higashi-Hiroshima 724, Japan*
[13] *University of Illinois, Urbana, Illinois 61801*
[14] *Institute of Particle Physics, McGill University, Montreal H3A 2T8, and University of Toronto, Toronto M5S 1A7, Canada*
[15] *The Johns Hopkins University, Baltimore, Maryland 21218*
[16] *Institut für Experimentelle Kernphysik, Universität Karlsruhe, 76128 Karlsruhe, Germany*
[17] *National Laboratory for High Energy Physics (KEK), Tsukuba, Ibaraki 305, Japan*
[18] *Ernest Orlando Lawrence Berkeley National Laboratory, Berkeley, California 94720*
[19] *Massachusetts Institute of Technology, Cambridge, Massachusetts 02139*
[20] *University of Michigan, Ann Arbor, Michigan 48109*
[21] *Michigan State University, East Lansing, Michigan 48824*
[22] *University of New Mexico, Albuquerque, New Mexico 87131*
[23] *The Ohio State University, Columbus, Ohio 43210*
[24] *Osaka City University, Osaka 588, Japan*
[25] *Universita di Padova, Istituto Nazionale di Fisica Nucleare, Sezione di Padova, I-35131 Padova, Italy*
[26] *University of Pennsylvania, Philadelphia, Pennsylvania 19104*
[27] *Istituto Nazionale di Fisica Nucleare, University and Scuola Normale Superiore of Pisa, I-56100 Pisa, Italy*
[28] *University of Pittsburgh, Pittsburgh, Pennsylvania 15260*
[29] *Purdue University, West Lafayette, Indiana 47907*
[30] *University of Rochester, Rochester, New York 14627*
[31] *Rockefeller University, New York, New York 10021*
[32] *Rutgers University, Piscataway, New Jersey 08855*
[33] *Academia Sinica, Taipei, Taiwan 11530, Republic of China*
[34] *Texas A&M University, College Station, Texas 77843*
[35] *Texas Tech University, Lubbock, Texas 79409*
[36] *Istituto Nazionale di Fisica Nucleare, University of Trieste/Udine, Italy*
[37] *University of Tsukuba, Tsukuba, Ibaraki 315, Japan*
[38] *Tufts University, Medford, Massachusetts 02155*
[39] *Waseda University, Tokyo 169, Japan*
[40] *University of Wisconsin, Madison, Wisconsin 53706*
[41] *Yale University, New Haven, Connecticut 06520*

(17 March 1998)

Abstract

We report the observations of the decays $B^+ \to \psi(2S)\,K^+$ and $B^0 \to \psi(2S)\,K^*(892)^0$ in $p\bar{p}$ collisions at a center-of-mass energy of 1.8 TeV using a 110 pb^{-1} data sample recorded by the Collider Detector at Fermilab. We also reconstruct the decays $B^+ \to J/\psi\,K^+$ and $B^0 \to J/\psi\,K^*(892)^0$ and measure the six ratios of branching fractions of these four decays. The relative branching-fraction results are shown to be consistent with phenomenological factorization calculations of hadronic B-meson decays. We use the world-average branching fraction $\mathcal{B}(B^+ \to J/\psi\,K^+)$ to derive $\mathcal{B}(B^+ \to \psi(2S)\,K^+) = (0.56 \pm 0.08 \pm 0.10) \times 10^{-3}$, $\mathcal{B}(B^0 \to \psi(2S)\,K^*(892)^0) = (0.92 \pm 0.20 \pm 0.16) \times 10^{-3}$, and $\mathcal{B}(B^0 \to J/\psi\,K^*(892)^0) = (1.78 \pm 0.14 \pm 0.29) \times 10^{-3}$, where the first and second uncertainties are statistical and systematic, respectively.

PACS Numbers: 13.25.Hw, 13.87.Fh, 14.40.Nd

Typeset using REVTEX

I. INTRODUCTION

Studies of the decays of bound states of bottom quarks and light antiquarks have proven to be one of the most effective ways to explore the decay dynamics of heavy quark systems. The branching fractions ($\mathcal{B}$) of the decays of the two lowest-lying bound states, the B^+ and B^0 mesons, depend on a blend of effects due to the weak and strong interactions. The measurements of semileptonic decays of B mesons, where a charged lepton and its corresponding neutrino are produced, have proven to be useful in the development of theoretical models that relate the semileptonic branching fractions to each other [1]. In a similar way, the measurements of the fully hadronic decays (modes where the B-meson decay daughters are hadrons) have also been shown to provide tests of the theory of heavy quark decay [2,3].

In this paper, we report the observations of the decays $B^+ \to \psi(2S)\,K^+$ and $B^0 \to \psi(2S)\,K^*(892)^0$ in $p\bar{p}$ collisions at a center-of-mass energy of 1.8 TeV. We also observe the decays $B^+ \to J/\psi\,K^+$ and $B^0 \to J/\psi\,K^*(892)^0$ and use our data to measure the ratios of branching fractions of the B^+ and B^0 mesons to these four final states. We compare our measurements with theoretical branching-fraction ratio predictions. Throughout this paper, references to a specific decay mode imply the charge conjugate mode as well.

As illustrated in the diagram in Fig. 1, all four of the J/ψ and $\psi(2S)$ decay modes are color-suppressed Cabibbo-favored decays; they can only occur when the W boson's hadronic decay products, themselves a color singlet, combine with the charm antiquark from the flavor-changing decay and the light spectator quark to form color-singlet charmonium and strange mesons, respectively. Strong interaction effects, however, are expected to modify the dynamics of these decays. The most successful theoretical treatments of such decays employ the factorization hypothesis, where the decay of the B meson is described by processes that take place on different time scales: short-distance hard-gluon exchange and the weak nonleptonic decay of the b quark, followed by longer-distance strong interactions between the final-state partons that produce the two daughter mesons. The decay amplitude is factorized into a product of hadronic currents that reduces to the charmonium decay constant and the matrix element for the $B \to K$ hadronic current, which consists of several form factors [1,2]. Measurements of the rates and polarization of these decays confront the assumptions that underlie the factorization hypothesis in B-meson decays and the calculations involving hadronic form factors.

Exclusive hadronic decays of B mesons are difficult to observe due to their relatively small branching fractions (typically 10^{-4} to 10^{-2}) and the small exclusive branching fractions of the subsequent charm daughter decays. However, the large production cross section for bottom quarks in $p\bar{p}$ collisions (in the range of 2-3 μb for quarks with transverse momentum $P_T > 6$ GeV/c and rapidity $|y_b| < 1$) has made it possible to identify relatively large samples of specific decay modes [4]. The decay modes that involve a charmonium daughter meson have proven to be most amenable to study, as the decay of the charmonium state involving two energetic muons yields a distinctive signature that can be used to identify the candidate events. The Collider Detector at Fermilab (CDF) Collaboration has published a number of measurements of the properties of B mesons using final states involving a J/ψ meson, including production cross sections, masses, lifetimes, polarizations, and branching fractions [4–8].

The CDF Collaboration measured the branching fractions of B^+, B^0, and B_s^0 mesons

using five different decay modes, all identified by requiring a $J/\psi \to \mu^+\mu^-$ decay [8]. We have now completed a more extensive study, incorporating a factor of four more data and focusing on the final states identified by the presence of a decay of the form

$$\begin{aligned} B \to \psi(2S)\, K \\ \hookrightarrow \mu^+\,\mu^- \\ \hookrightarrow J/\psi\, \pi^+\,\pi^- \\ \hookrightarrow \mu^+\,\mu^-, \end{aligned} \tag{1}$$

where B is a B^+ (B^0) meson and K is a K^+ ($K^*(892)^0$) meson. The $K^*(892)^0$ meson is observed through its decay to the $K^+\pi^-$ final state.

We first describe in Secs. II and III the experiment and data-collection procedures used for this measurement. In Sec. IV, we discuss the event selection procedure and present the observed rates of the various B-meson decays. The necessary efficiency corrections to convert the observed decay rates to branching fractions are discussed in Sec. V where we also detail the systematic uncertainties associated with the measurement. We present our results in Sec. VI and offer our conclusions in Sec. VII.

II. EXPERIMENTAL APPROACH

In principle, the number of observed events for the decay mode $B^+ \to \psi(2S)\, K^+$ can be decomposed into the form

$$N_{\rm obs}(\psi(2S)\, K^+) = 2 \int \mathcal{L} dt \cdot \sigma(p\bar{p} \to \bar{b}) \cdot f_u \cdot \mathcal{B}(B^+ \to \psi(2S)\, K^+) \cdot \epsilon^{\psi(2S)\, K^+}, \tag{2}$$

and similar forms can be written for the other decays. Here, $\int \mathcal{L} dt$ is the time-integrated luminosity, $\sigma(p\bar{p} \to \bar{b})$ is the bottom antiquark production cross section, and f_u is the probability that the fragmentation of a bottom antiquark will result in a B^+ meson. In a similar way, we define f_d to be the probability of a bottom antiquark to hadronize and form a B^0 meson. We refer to these probabilities as fragmentation fractions and include in these fractions contributions from decays of heavier bottom hadrons into final states containing a B^+ or B^0 meson. The expression $\mathcal{B}(B^+ \to \psi(2S)\, K^+)$ represents the branching fraction for this B^+-meson decay mode, and $\epsilon^{\psi(2S)\, K^+}$ is the acceptance and efficiency of detecting the $\psi(2S)\, K^+$ final state. The factor of 2 accounts for the possibility of reconstruction of B^- or B^+ mesons in each event.

The observation of a certain number of B-meson decays in a specific mode can be converted into a branching-fraction measurement using an expression similar to Eq. (2). However, uncertainties in the bottom-quark production cross section [4] can be avoided by measuring ratios of branching fractions between B-meson decay modes, a procedure that also results in the beneficial cancellation of several detection and reconstruction efficiencies and their associated uncertainties. For example, a branching-fraction ratio involving only J/ψ charmonium mesons is measured as

$$\frac{\mathcal{B}(B^0 \to J/\psi\, K^*(892)^0)}{\mathcal{B}(B^+ \to J/\psi\, K^+)} = \frac{N_{\rm obs}(J/\psi\, K^*(892)^0) \cdot f_u \cdot \epsilon^{J/\psi\, K^+}}{N_{\rm obs}(J/\psi\, K^+) \cdot f_d \cdot \epsilon^{J/\psi\, K^*(892)^0} \cdot \mathcal{B}(K^*(892)^0 \to K^+\,\pi^-)}, \tag{3}$$

where $N_{\rm obs}(J/\psi\, K^*(892)^0)$ and $N_{\rm obs}(J/\psi\, K^+)$ denote the observed event yields and $\epsilon^{J/\psi K^*(892)^0}$ and $\epsilon^{J/\psi K^+}$ represent the detector acceptance and reconstruction efficiencies, which have several common factors, such as the J/ψ branching fraction and reconstruction efficiency, that divide out of the ratio. Ratios of branching fractions are also beneficial in theoretical studies of these decays since several common factors divide out of the amplitude expressions [9,10].

These ratios of branching fractions can be used to estimate absolute branching fractions using world-average values for the denominator of the ratios. This is particularly useful for those ratios that involve the most precisely known branching fraction, $\mathcal{B}(B^+ \to J/\psi\, K^+)$, in the denominator. We use the world-average value of $\mathcal{B}(B^+ \to J/\psi\, K^+)$ to estimate the absolute branching fractions of the other three decay modes.

III. DATA COLLECTION

A. The CDF Detector

The Collider Detector at Fermilab is a multi-purpose detector designed to study 1.8 TeV $p\bar{p}$ collisions produced by the Fermilab Tevatron collider [11]. The detector has a coordinate system with the z axis along the proton beam direction, the y axis pointing vertically upwards, and the x axis pointing horizontally. The polar angle θ is defined relative to the z axis and ϕ is the azimuthal angle. Pseudorapidity is defined as $\eta \equiv -\ln[\tan(\theta/2)]$. The CDF detector surrounds the interaction region with three charged-particle tracking detectors immersed in a 1.4 T solenoidal magnetic field. The tracking system is contained within a calorimeter system that measures the energy flow of charged and neutral particles out to $|\eta| < 4.2$. Charged-particle detectors outside the calorimeter are used to identify muon candidates.

The innermost tracking device is a silicon microstrip detector (SVX) located in the region between 2.9 and 7.9 cm in radius from the beam axis. The SVX is surrounded by a set of time projection chambers (VTX) that measure charged-particle trajectories to a radius of 22 cm. An 84 layer drift chamber (CTC) measures the particle trajectories in the region between 30 and 132 cm in radius from the beam. This tracking system has high efficiency for detecting charged particles with momentum transverse to the beam $P_T > 0.35$ GeV/c and $|\eta| \lesssim 1.1$. Together, the CTC and SVX measure charged-particle transverse momenta with a precision of $\sigma_{P_T} \simeq [(0.0066 P_T)^2 + (0.0009 P_T^2)^2]^{1/2}$ (with P_T in units of GeV/c).

The muon detection system has four of its layers of planar drift chambers separated from the interaction point by approximately five interaction lengths of material. To reduce the probability of misidentifying penetrating hadrons as muon candidates in the central pseudorapidity region $|\eta| < 0.7$, four more layers of chambers are located outside the magnet return yoke (corresponding to a further three interaction lengths of material at $\theta = 90°$). An additional set of chambers is located in the pseudorapidity interval $0.7 < |\eta| < 1.0$ to extend the polar acceptance. The muon system is capable of detecting muons with $P_T \gtrsim 1.4$ GeV/c in a pseudorapidity interval $|\eta| < 1.0$. A three-level trigger system is used to select candidate collisions for subsequent study. These and other elements of the CDF detector are described in more detail elsewhere [11].

B. The Data Set

The data were collected in two running periods, the first extending for nine months starting in August 1992, and the second extending for 18 months starting in January 1994. Several modifications were made to the CDF detector during the hiatus between these two running periods. The most significant of these were the replacement of the silicon microstrip detector, the commissioning of a trigger system with greater selectivity, and improvements to the data acquisition system. The most notable difference in running conditions resulted from a rise in the average instantaneous luminosity of the Tevatron accelerator. The mean instantaneous luminosities during the two periods were 3.5×10^{30} cm^{-2}s^{-1} and 8.0×10^{30} cm^{-2}s^{-1}, respectively, and the peak instantaneous luminosity exceeded 2.0×10^{31} cm^{-2}s^{-1}. The time-integrated luminosity of the data sample for the two running periods is $\sim$20 pb^{-1} and $\sim$89 pb^{-1}, respectively.

Despite the differences in detector configuration during the two running periods, we were able to treat the two sets of data as a single sample with a total time-integrated luminosity of $\sim$109 pb^{-1}. This was achieved through the use of nearly identical event reconstruction techniques and consistent calibration procedures for data collected during the two running periods.

IV. EVENT SELECTION

A. The J/ψ and $\psi(2S)$ Trigger Requirements

A common feature of the four B-meson decay modes studied here is the presence of a $\mu^+\mu^-$ candidate consistent with that arising from the decay of a charmonium (J/ψ or $\psi(2S)$) state.

We used a three-level trigger system to identify collisions producing two or more muon candidates. The first-level trigger required that two muon candidates be observed in the muon system. The first-level trigger track efficiency in the muon system rose from $\sim$40% at $P_T = 1.5$ GeV/c to $\sim$93% for muons with $P_T > 3.0$ GeV/c. The second-level trigger required the detection of at least one charged track in the CTC using the central fast track processor (CFT) [12], which performed a partial reconstruction of all charged tracks with a transverse momentum exceeding $\sim$2 GeV/c. The CFT track was required to match within $\sim 8^\circ$ in ϕ of the muon candidate. The CFT efficiency rose from $\sim$40% at a muon $P_T \sim 2$ GeV/c to $\sim$94% for $P_T \gtrsim 3$ GeV/c. The third-level trigger required that two reconstructed CTC tracks be matched with two tracks in the muon chambers and that the invariant mass of the dimuon pair be between 2.7 and 4.1 GeV/c^2. The efficiency of the third-level trigger requirement was (97 ± 2)% for J/ψ decays passing the first and second-level triggers. Deviations from these nominal trigger efficiencies were observed to occur during data acquisition and were taken into account in our study. There are 3.1×10^6 dimuon candidate events that passed the third-level trigger requirements.

Since the average energy deposition of a muon passing through the calorimeter system into the muon chambers was 1.4 GeV, we required that all muon candidates have $P_T >$ 1.4 GeV/c; however, more stringent criteria on the P_T of the muon candidates were imposed by the three-level trigger system, which effectively placed a P_T threshold of approximately

2 GeV/c on each of the two muon candidates. The momentum selection of muon candidates by the trigger enhanced the signal yield without introducing large systematic uncertainties, since the trigger efficiency was precisely measured.

In approximately 75% of our selected events, the two muon candidates that were identified as charmonium daughters were also the muon candidates identified by the dimuon trigger system. In many of the remaining events, an additional muon candidate in the event satisfied the dimuon trigger requirements. We included these "volunteers" in our analysis in order to maximize the sensitivity of the data sample.

B. Primary-Vertex and Charged-Particle Reconstruction

We first identified the location of the $p\bar{p}$ interaction vertex or vertices using the observed tracks reconstructed in the VTX detector. These tracks, when projected back to the beam axis, determined the longitudinal locations of these interactions. Due to the high instantaneous luminosities, the number of reconstructed interaction vertices in a given event follows a Poisson distribution with a mean of $\sim$2.5. We chose as the longitudinal position of the primary $p\bar{p}$ collision vertex for the dimuon candidates the interaction vertex that was closest to either one of the muon candidates' intercepts along the beamline. This provided a measurement of the primary vertex position with an accuracy of 0.3 cm along the beam direction.

The transverse position of the primary vertex was most accurately determined by using the average beam position through the detector and the longitudinal primary vertex position. The average trajectory was stable over the period that a given $p\bar{p}$ beam was stored in the Tevatron. The uncertainty in the transverse position of the primary vertex was dominated by the transverse size of the beam, which was 25 μm in both the x and y directions.

Candidate μ^+, K^+, and π^+ trajectories were reconstructed in the CTC and extrapolated into the SVX detector to identify hits associated with the given track. We required each CTC track candidate to be of high quality by stipulating that a candidate track have a minimum number of hits in the CTC. We also required that additional SVX information consist of at least two out of a possible four hits (for the earlier of the two running periods, at least three hits were required). The CTC tracks were also required to pass through most of the active volume of the CTC; this was imposed by demanding that the radius of exit from the CTC volume of the charged-track trajectory be at least 110 cm. We also required that K^+ and π^+ candidates have a measured transverse momentum $P_T > 0.4$ GeV/c in order that they be reconstructed reliably.

C. Event Topology Reconstruction

We performed an event reconstruction using the muon and charged-track candidates. The first step of this procedure was to reconstruct a candidate charmonium decay to the dimuon final state. The second step was to associate additional tracks with the charmonium candidate to form a candidate B-meson decay. During this process, we made various selection requirements, described below, to reduce the combinatorial backgrounds and to improve the signal-to-noise ratio for the various decay modes.

1. Reconstruction of J/ψ and $\psi(2S)$ Decays

In order to reduce the rate of muon candidates from background sources such as K-meson decay-in-flight, we required that each muon candidate observed in the muon chambers correspond to a CTC track candidate to within three standard deviations of the multiple-scattering and measurement uncertainties in both the transverse and longitudinal planes.

Backgrounds in the dimuon sample were further reduced by performing a least squares fit of the CTC tracks associated with the muon candidates under the constraint that they originate from a common vertex. We required that the confidence level of this fit be greater than 0.01. The dimuon mass distributions for the J/ψ and $\psi(2S)$ candidates are shown in Fig. 2. We fit these distributions to parametrized signal and background lineshapes to determine that our sample consists of $(4.39 \pm 0.01) \times 10^5$ J/ψ decays and $(1.31 \pm 0.04) \times 10^4$ $\psi(2S)$ decays, where we quote only the statistical uncertainties. Candidate dimuon events were fit with the additional constraint that the two-muon mass equal the world-average masses [13] of the J/ψ and $\psi(2S)$ mesons, 3.09688 and 3.68600 GeV/c^2, respectively. We required that the confidence level of this fit exceed 0.01. This requirement defined our inclusive J/ψ and $\psi(2S)$ data sets.

Candidates for the decay $\psi(2S) \to J/\psi\,\pi^+\pi^-$ were identified by combining every J/ψ candidate identified above with pairs of oppositely-charged track candidates that individually had to have $P_T > 0.4$ GeV/c. The two-particle mass of the two pion candidates was required to satisfy $0.35 < M(\pi^+\pi^-) < 0.61$ GeV/c^2. The lower limit of this mass range was motivated by the known dipion mass distribution for $\psi(2S)$ decays [14–17]. The upper limit corresponded to the maximum dipion mass allowed for $\psi(2S)$ decays. The efficiency of this criterion to select $\psi(2S)$ decays is demonstrated in Fig. 3, where we plot the two-pion mass for observed $\psi(2S) \to J/\psi\,\pi^+\pi^-$ decays. The background to the $\psi(2S)$ decays in this distribution has been removed by performing a sideband subtraction using background events in the $J/\psi\,\pi^+\pi^-$ mass distribution. Also shown are curves representing a phenomenological prediction [17] and a pure phase-space calculation.

To reduce combinatorial backgrounds in the $J/\psi\,\pi^+\pi^-$ candidate search further, an additional least-squares fit was performed constraining all four tracks to emanate from a common point, the dimuon mass to be equal to the world-average J/ψ mass, and the $J/\psi\,\pi^+\pi^-$ mass to be equal to the world-average $\psi(2S)$ mass. We required that the confidence level for this fit exceed 0.01. The $J/\psi\,\pi^+\pi^-$ mass distribution for all the candidates prior to imposing the $\psi(2S)$ mass constraint is shown in Fig. 4 and illustrates a narrow $\psi(2S)$ signal of $(3.7 \pm 0.1) \times 10^3$ events above the combinatorial background.

Our subsequent reconstruction identified K^+ and π^+ meson candidates that were consistent with arising from one of the four B-meson decay modes we considered in this study.

2. Reconstruction of B-Meson Exclusive Decays

The reconstruction of the B-meson decay modes required the use of selection criteria that reduced the potentially large combinatorial background. The most effective way of reducing these backgrounds was to impose minimum P_T requirements on the candidate strange-meson daughters, P_T requirements on the B-meson candidates, and requirements

that the decay topology be consistent with that expected from a B-meson decay. Explicit particle identification of K^+ and π^+ mesons was not employed in this analysis.

These additional requirements imposed on the candidates were also selected to be as common as possible over the four B-meson decay channels and both decay modes of the $\psi(2S)$ meson to avoid significant systematic uncertainties arising from the estimation of B-meson yields across different kinematic regions. The kinematic selection criteria were optimized by maximizing the quantity $N_s/\sqrt{N_s + N_b}$, where N_s was the predicted number of signal events based on Monte Carlo calculations and N_b was the number of observed background events in the B-meson mass signal region estimated by performing extrapolations from the sideband regions. This technique avoided the potential bias that could be introduced by choosing selection criteria based on the number of observed candidate signal events.

We required that each K^+ candidate have $P_T > 1.5$ GeV/c for the reconstruction of B^+ candidates. For the reconstruction of B^0 candidates, we required that the $K^*(892)^0$ candidate have $P_T > 2.0$ GeV/c. In the latter case, the K^+ and π^- daughters from the $K^*(892)^0$ decay were required to have $P_T > 0.4$ GeV/c. In the $K^*(892)^0$ reconstruction, all possible charged-particle candidate pairs were considered with both mass assignments. A track-pair mass assignment was considered a candidate $K^*(892)^0$ decay if the two-particle mass was within 0.0800 GeV/c^2 of the world-average $K^*(892)^0$ mass of 0.8961 GeV/c^2. For a small fraction of the track-pair candidates, it was possible that both the $K^+\pi^-$ and π^+K^- mass assignments fell within this mass window around the $K^*(892)^0$ pole, resulting in double counting of signal events. This double counting was taken into account using a Monte Carlo calculation described below.

To identify B-meson candidates, a least-squares fit was performed on the charged-particle tracks associated with the charmonium and strange-meson candidates, constraining them to originate from a common decay point with the charmonium-candidate mass constraints described above. In addition, this fit constrained the momentum vector of the B-meson candidate to be parallel to its flight path, defined by the measured production and decay points, in the transverse plane and required that the B candidate originate from the primary interaction vertex. We required the confidence level of this fit to exceed 0.01. We also required that the transverse momentum of the B^+ candidates be greater than 6.0 GeV/c and the transverse momentum of the B^0 candidates be greater than 9.0 GeV/c. These different B-meson P_T selection criteria constitute the largest difference in the kinematic requirements between decay modes involving B^+ and B^0 final states and are a result of the different levels of combinatorial background in the $\psi(2S)$ final states.

Two additional criteria were imposed to reduce combinatorial backgrounds further. In the fragmentation of b quarks into B mesons, the meson typically carries most of the energy of the quark created in the hard scattering interaction [18]. We exploit this fact to suppress backgrounds by defining an isolation variable

$$I_B \equiv \frac{\sum_i \vec{P}_i \cdot \vec{P}_B}{|\vec{P}_B|^2}, \tag{4}$$

where the sum is over charged particles with momentum vectors $\vec{P}_i$, contained within a cone in η-ϕ space of radius $R \equiv \sqrt{(\Delta\phi)^2 + (\Delta\eta)^2} = 1.0$ about an axis defined by the direction of

the B-candidate momentum $\vec{P}_B$. Track candidates belonging to the B-meson candidate were not included in this sum. In order to avoid including charged particles that resulted from interactions in the $p\bar{p}$ collision not associated with the B-meson candidate, we made the sum over only those charged-particle tracks that passed within 5 cm along the z axis of the primary interaction location. We expect B-meson decays to have relatively small values of I_B, and therefore imposed the requirement $I_B < 0.54$, which resulted from the optimization procedure. We show in Fig. 5 the distribution of I_B for $B^+ \to J/\psi\, K^+$ candidate decays, after statistically subtracting the combinatorial background under the B^+ decay signal using background events in the $J/\psi\, K^+$ mass-sideband regions. This illustrates that the B-meson decays are efficiently identified by this requirement.

As a final B-meson selection requirement, we exploited the relatively long lifetimes of B mesons and the excellent secondary vertex resolution of the CDF detector to reject those events that have short decay lengths [6]. We measured the proper decay length for each decay candidate,

$$c\tau_B \equiv \frac{\vec{P}_T \cdot \vec{x}_T}{P_T^2}\, m_B, \tag{5}$$

where m_B is the mass of the B-meson candidate, $\vec{x}_T$ is the flight path measured in the transverse plane, and $\vec{P}_T$ is the B-meson vector transverse momentum. The $c\tau_B$ resolution depended primarily on the number of track candidates possessing SVX hit information. We required that $c\tau_B > 100\ \mu$m.

D. B-Meson Signals

The candidate mass distributions for the $B^+ \to J/\psi\, K^+$ and $B^+ \to \psi(2S)\, K^+$ decays are shown in Fig. 6. The mass distributions for the $B^0 \to J/\psi\, K^*(892)^0$ and $B^0 \to \psi(2S)\, K^*(892)^0$ decays are shown in Fig. 7. We see signal peaks at the B^+ and B^0 masses in all six decay modes. The distributions describing the $\psi(2S)$ final states constitute the first observations of these modes in $p\bar{p}$ collisions. To obtain the yield of B^+ candidates, each distribution was fit to a Gaussian signal lineshape with a linear background parametrization using a binned maximum likelihood technique. The fits were performed over the B-meson candidate mass region from 5.15 GeV/c^2 to 5.60 GeV/c^2. The lower edge of this range was chosen to avoid possible biases from incompletely reconstructed B-meson decay modes where one or more decay daughters went undetected.

For the B^0 candidates, a single Gaussian lineshape did not accurately describe the signal due to ambiguities in the $K^*(892)^0$ daughter (K^+ and π^- mesons) mass assignments in approximately 25% of the signal events. To correct for this effect, we used a Monte Carlo calculation to determine the lineshape for the correct and incorrect mass assignments and found that each of these was accurately described with a Gaussian parametrization centered on the nominal B^0 mass. The width of the mass distribution arising from the wrong mass assignment was 4-6 times broader than the width of the mass distribution associated with the right mass assignment, although the parametrization differed for the three different B^0 decay modes. We list the ratio of the peak amplitudes of the wrong versus right mass combinations and the ratio of the widths of these two Gaussians in Table I. The signal yields, masses, and resolutions of the B^+ and B^0 candidates are summarized in Table II.

V. ACCEPTANCE AND EFFICIENCY MEASUREMENTS

We used a Monte Carlo calculation of b-quark production and B-meson decay, followed by a detailed detector simulation to study and measure the kinematic and geometric acceptances for each decay mode. We used data to estimate the remaining efficiencies associated with the reconstruction algorithms and the event selection criteria.

An advantage of measuring ratios of branching fractions for similar decay modes is that many of the acceptances and efficiencies cancel in the numerator and denominator; however, there are several effects that do not cancel completely and have associated with them systematic uncertainties that differ depending on which channels are being compared. Examples of these include the effect of the decay-length requirement and the polarization of the B-meson decay to vector-vector final states. We have taken these into account and arrived at separate estimates of systematic uncertainties for each of the six ratios that were measured.

A. Acceptance and Trigger Efficiency Measurements

The Monte Carlo calculation used a model for b-quark production based on a next-to-leading-order QCD calculation [19]. This calculation employed the Martin-Roberts-Stirling set D0 (MRSD0) parton distribution functions [20] to model the kinematics of the initial-state partons; a value for the b-quark mass of $m_b = 4.75$ GeV/c^2; and a renormalization scale of $\mu = \mu_0 \equiv \sqrt{m_b^2 + k_T^2}$, where k_T is the momentum of the b quark in the plane transverse to the directions of the incoming protons. We generated b quarks in the rapidity interval $|y_b| < 1.1$ and with $k_T > 5.0$ GeV/c. These generator limits were chosen so that there were no biases in the B-meson kinematic distributions after the application of the kinematic cuts used in this analysis. The b quarks were fragmented into B mesons according to the Peterson fragmentation function [18] with the parameter ϵ_b defined to be 0.006 [21].

The generated B mesons were decayed into the various final states using two-body decay kinematics governed by the world-average masses and lifetimes of the daughter particles [13]. For the $\psi(2S) \to J/\psi\, \pi^+ \pi^-$ mode, the decay matrix element used was the Pham *et al.* model [17,22], a parametrization of which is shown in Fig. 3.

For the $J/\psi\, K^*(892)^0$ and $\psi(2S)\, K^*(892)^0$ decays, which involve two vector mesons in the final state, we used the world-average longitudinal polarization for the $J/\psi K^*(892)^0$ decay, $\Gamma_L/\Gamma = 0.78 \pm 0.07$ [3]. The polarization has not been measured in $B^0 \to \psi(2S)\, K^*(892)^0$ decays; therefore, we use the value of Γ_L/Γ for the $B^0 \to J/\psi\, K^*(892)^0$ decay but double the uncertainty to ± 0.14.

The resulting generated events were passed through a detailed simulation of the CDF detector that took into account decays-in-flight, the geometry of all the subdetector elements, the interaction of the charged particles with the material in the detector, the resolution of the different tracking elements, and the efficiency of the trigger.

We used a parametrization of the muon-P_T dependence of our first and second-level trigger system to determine the trigger efficiency for the various B-meson decays in which the muons that resulted from the charmonium decay were also identified by the trigger's dimuon selection criteria. In the remaining events, which corresponded to approximately 25% of the selected event sample, an additional muon candidate in the event often satisfied the dimuon trigger requirements. This led to a $\sim$5% uncertainty in the topology dependence

of the relative trigger efficiency. We included this as a separate systematic uncertainty in our branching-fraction measurements.

The resulting geometric acceptances for the different decay modes are presented in Table III, where we list the fraction of decays expected to contribute to the observed signal peak.

B. Reconstruction Efficiencies

The efficiencies of the subdetectors and reconstruction algorithms used in this analysis to identify charged-particle candidates and reject backgrounds were separately estimated using information from the collected data together with Monte Carlo calculations. The use of data that properly represented the running conditions experienced at the Tevatron Collider was particularly important in cases where these efficiencies were expected to depend on the instantaneous luminosity.

1. Track Reconstruction Efficiency

Because of the different number of charged particles used in the reconstruction of each of the exclusive decay modes in this analysis, we had to estimate the efficiency of the track reconstruction algorithms when reconstructing three, four, five, or six-prong decays. The large number of charged particles associated with an interaction producing a B meson (typically $\sim$40 charged particles in the fiducial region of the CTC) and the large number of simultaneous interactions created very high hit occupancies in the innermost layers of the CTC, reducing their effectiveness.

We measured the efficiency of the CTC track-finding algorithm by embedding the wire hits from one or two Monte Carlo charged-particle tracks into a set of data events identified as having a J/ψ candidate. This event sample was selected to be representative of the inclusive J/ψ and $\psi(2S)$ data set, taking into account variations in detector configuration and instantaneous luminosity. Our embedding procedure used the hit detection efficiencies and resolutions observed in the data to simulate the response of the CTC. We then used the standard track reconstruction algorithms to seek a reconstructed track helix that formed a match with the embedded particle's trajectory. The track matching criterion was imposed on a χ^2 variable with five degrees of freedom that accounted for parameter correlations and measurement uncertainties by employing in its definition the covariance matrix of the reconstructed track helix. For an embedded Monte Carlo track in a data event, χ^2 values were computed for all of the reconstructed tracks in the event. A track was deemed to be a match if it had the lowest χ^2 of all tracks in the event and if this χ^2 value was $<$500, a highly efficient requirement.

We measured the efficiency for reconstructing a $\pi^\pm$ meson as a function of the meson's P_T, shown in Fig. 8, and as a function of several other variables [23]. We found the average efficiency for $\pi^\pm$ mesons to be $0.928 \pm 0.003 \pm 0.026$ for meson $P_T > 0.4$ GeV/c, where the quoted uncertainties are statistical and systematic, respectively. Because of the use of the decay mode $\psi(2S) \to J/\psi\, \pi^+\, \pi^-$, which introduced two additional charged tracks, we also repeated this procedure by embedding pairs of charged tracks in each real event. We found the

efficiency for reconstructing the two daughter pion tracks in the decay $\psi(2S) \to J/\psi\,\pi^+\,\pi^-$ to be $0.881 \pm 0.005 \pm 0.043$. The systematic uncertainties in these two measurements are largely correlated because they were dominated by the uncertainty in the CTC hit efficiencies used in the track embedding procedure. Since the square of the single-track efficiency is substantially smaller than the two-track reconstruction efficiency, we concluded that the track-finding efficiencies of several charged particles in a single event were correlated, an effect that was taken into account in our subsequent efficiency calculations.

2. Requirements on the Fits to Decay Topologies

We measured the efficiencies of the constrained-fit confidence-level criteria for the different decay topologies using the observed J/ψ and $\psi(2S)$ signal yields before and after making the confidence-level requirements discussed in Sec. IV C. These comparisons resulted in efficiencies for the constrained fits to the $J/\psi \to \mu^+\,\mu^-$ and the $\psi(2S) \to \mu^+\,\mu^-$ decay hypotheses that were equal within uncertainties. The efficiency for satisfying the confidence-level requirement on the fit employing a vertex constraint was 0.967 ± 0.003 and the efficiency for the fit employing the additional charmonium mass constraint was 0.963 ± 0.002. Since these efficiencies do not depend on the charmonium parent, they cancel in the measurement of the ratios of branching fractions. The uncertainty in these measurements arises from the finite statistics of the two charmonium samples.

The third charmonium topology, $\psi(2S) \to J/\psi\,\pi^+\,\pi^-$, includes two low-momentum charged pions in the decay vertex in addition to the muons. We measured the extra inefficiency caused by the vertex-constrained fit to this decay by measuring the loss of $\psi(2S)$ signal events when making the confidence-level requirement. This resulted in a correction factor of 0.834 ± 0.039 for the efficiency of the requirement on the vertex fit alone and a factor of 0.945 ± 0.031 corresponding to the additional mass-constrained fit requirement.

3. Decay-Length Requirement

The efficiencies of the B-meson decay-length requirement on the different decay modes discussed in Sec. IV C were measured by modeling the decay-length resolution, which was determined by the number of tracks reconstructed in the SVX detector, and using the world-average lifetimes for the B^+ and B^0 mesons [13]. We determined the decay-length resolutions for events with different numbers of SVX tracks using B-meson candidate events outside of the signal mass region. We then used the Monte Carlo calculation and detector simulation to estimate the expected frequencies of events with different numbers of SVX tracks. These were then convolved together with the expected exponential decay-length distributions for each B-meson species to obtain a prediction for the observed decay-length distributions.

The efficiencies of the decay-length requirement were $\sim$0.75 and varied only slightly between decay modes. The uncertainties in these efficiencies were dominated by uncertainties in the world-average B-meson lifetimes [13] and in the number of candidate daughter tracks with SVX hit information.

4. Isolation Requirement

The B-meson isolation criterion I_B discussed in Sec. IV C rejected combinatorial background. The efficiency of this selection requirement is 0.928 ± 0.054, which we measured by estimating the loss of B-meson decays when applying this criterion for each decay mode. We note, for example, that we improve the signal-to-noise ratio in the $J/\psi K^+$ channel by a factor of three when applying this criterion.

We assume that the isolation criterion is independent of the final-state topology. We do not expect this isolation requirement to depend on the specific B-meson final state, since it was defined using only the B-meson momentum and the momentum of the charged particles produced in the production and fragmentation of the b quark. We verified this by measuring the efficiencies independently in each channel, but the statistical power of this check is limited.

C. Relative Acceptance and Efficiency Corrections

For the purpose of determining relative branching fractions, the geometric and kinematic acceptance results listed in Table III were combined into twelve acceptance ratios involving the six reconstructed channels. Table IV provides a summary of these relative acceptances and their systematic uncertainties. The uncertainties include contributions from the following sources: finite Monte Carlo statistics, variations in the Monte Carlo P_T spectrum with changes in the renormalization scale and b-quark mass, modeling effects in the simulation of the second-level trigger, variations in the assumed longitudinal polarization fractions for the decays with vector-vector final states, and the uncertainty in the CDF detector simulation.

Table V is similarly structured to present the ratios of the products of the remaining efficiencies described in Sec. V B, namely those associated with track reconstruction, the constrained-fit confidence-level criteria, and the proper decay-length requirement.

VI. RESULTS

We present our results as six ratios of acceptance-corrected rates of B-meson decays into the four channels. In ratios involving $\psi(2S)$ mesons, the results for the two $\psi(2S)$ decay modes were combined, taking into account the $\psi(2S)$ branching fractions. The observed numbers of signal events for each decay, listed in Table II, were divided by the acceptance and reconstruction efficiencies listed in Tables IV and V, respectively. The event rates were also corrected for the daughter-meson branching fractions listed in Table VI. Additional systematic uncertainties of 4% and 2% were applied to the branching-fraction ratio calculations to account for uncertainties in the fitting technique used to estimate event yields and the lack of cancellation of the efficiencies of the B-candidate constrained-fit criteria, respectively. When we form the ratios of acceptance-corrected event rates, the b-quark production cross section, time-integrated luminosity, and common efficiencies divide out of the calculations. For both the B^+ and B^0-meson cases, we verified that the event rates for the two different $\psi(2S)$ decay modes were consistent after taking into account the differences in acceptance and reconstruction efficiencies.

The measured quantities are the ratios of the product of b-quark fragmentation fractions and the B-meson branching fractions into the specific final state. Thus, our measurements can be written as shown in Table VII, where the first uncertainty is statistical and the second uncertainty is the sum in quadrature of uncertainties in acceptance, efficiency, and the charmonium daughter branching fractions. This convention will be employed below unless otherwise noted. The ratio in Table VII involving exclusively the J/ψ decay mode has been measured previously with a subset of these data [8]. The present measurement supersedes it.

The results show that the rates of B-meson decays to the two $\psi(2S)$ final states are approximately 50% of the rates of the analogous decays to the J/ψ final states. In addition, we note that the relative rates of vector-vector decays to vector-pseudoscalar decays for the $\psi(2S)$ and J/ψ modes are the same to within relatively large statistical uncertainties. If we make the assumption [8,13] of equal fragmentation fractions, $f_u = f_d$, the vector-vector to vector-pseudoscalar decay rate for the J/ψ final states,

$$\frac{\mathcal{B}(B^0 \to J/\psi\, K^*(892)^0)}{\mathcal{B}(B^+ \to J/\psi\, K^+)} = 1.76 \pm 0.14 \pm 0.15, \tag{6}$$

is now the most precise single measurement of this quantity and provides a constraint on theoretical calculations that attempt to describe both this branching-fraction ratio and the longitudinal polarization of the vector-vector decay [7,9,10]. The analogous result for $\psi(2S)$ final states may be similarly obtained from Table VII.

A. Comparison with Phenomenological Models

We have compared the results of our measurements to two phenomenological predictions for these ratios based on the factorization hypothesis [1,2]. In this class of models, the ratios of branching fractions of J/ψ and $\psi(2S)$ decay modes depend largely on the strong interaction effects in the final state of each decay, which are modeled by sets of form factors specific to each decay. We have chosen two specific models [24,25], as predictions for the branching fractions for $\psi(2S)$ and J/ψ decays have been made using them.

The calculation by Neubert *et al.* [24] employs a set of form factors determined using a relativistic harmonic oscillator potential model for the meson wave functions and a dipole q^2 dependence for most of the form factors, where q^2 is the square of the four-momentum exchanged between the B meson and the daughter K meson. (The generic multipole form-factor formula is $F(q^2) = F(0)/(1 - q^2/m^2)^n$, where m is the pole mass and $n = 1$ or 2 for a monopole or dipole dependence, respectively.) The calculation by Deandrea *et al.* [25] determines the form factors empirically by extracting them from semileptonic D-meson decays and assuming that they have a monopole q^2 dependence.

The measured ratios of branching fractions are compared with these two theoretical calculations in Fig. 9, where we have assumed $f_u = f_d$. Both models are in agreement with the data. However, the results of Neubert *et al.* are favored overall by the data, whereas the calculation of Deandrea *et al.* predicts a lower branching fraction for the $B^+ \to \psi(2S)\, K^+$ decay.

B. Absolute Branching Fractions

We can use the world-average branching fraction [13]

$$\mathcal{B}(B^+ \to J/\psi\, K^+) = (1.01 \pm 0.14) \times 10^{-3} \tag{7}$$

and the assumption $f_u = f_d$ to convert our measurements of branching-fraction ratios into absolute branching-fraction measurements for the three other decay modes. There are no correlations between our data and the world-average value in Eq. (7), making the determination of the resulting uncertainties straightforward. We note that the world-average value is based on the assumption of equal f_u and f_d fragmentation fractions of b quarks produced in the decay of the $\Upsilon(4S)$ meson.

The derived branching fractions are therefore

$$\mathcal{B}(B^+ \to \psi(2S)\, K^+) = (0.56 \pm 0.08 \pm 0.10) \times 10^{-3} \tag{8}$$

$$\mathcal{B}(B^0 \to \psi(2S)\, K^*(892)^0) = (0.92 \pm 0.20 \pm 0.16) \times 10^{-3} \tag{9}$$

$$\mathcal{B}(B^0 \to J/\psi\, K^*(892)^0) = (1.78 \pm 0.14 \pm 0.29) \times 10^{-3}. \tag{10}$$

The first and second uncertainties are statistical and systematic, respectively.

The branching fractions for the $\psi(2S)$ decay modes are compared with previous measurements by the ARGUS [26], CLEO [27], and CLEO II [28] Collaborations in Fig. 10. The CDF results are in agreement with these previous measurements and have uncertainties that are approximately three times smaller. They represent a significant improvement in the knowledge of B-meson decays to $\psi(2S)$ final states. The $J/\psi\, K^*(892)^0$ branching fraction is also in good agreement with the world-average value [13] and a recent measurement published by the CLEO II Collaboration [29].

VII. CONCLUSION

We have made measurements of the rates of the exclusive decays

$$\begin{aligned} &B^+ \to \psi(2S)\, K^+ \\ &B^0 \to \psi(2S)\, K^*(892)^0 \\ &B^+ \to J/\psi\, K^+ \\ &B^0 \to J/\psi\, K^*(892)^0. \end{aligned} \tag{11}$$

Using the observed event rates, correcting for the relative efficiencies for these decay modes, and assuming equal fragmentation probabilities for B^+ and B^0 mesons, we measure the following ratios of branching fractions:

$$\frac{\mathcal{B}(B^0 \to J/\psi\, K^*(892)^0)}{\mathcal{B}(B^+ \to J/\psi\, K^+)} = 1.76 \pm 0.14 \pm 0.15$$

$$\frac{\mathcal{B}(B^+ \to \psi(2S)\, K^+)}{\mathcal{B}(B^+ \to J/\psi\, K^+)} = 0.558 \pm 0.082 \pm 0.056$$

$$\frac{\mathcal{B}(B^0 \to \psi(2S)\, K^*(892)^0)}{\mathcal{B}(B^+ \to J/\psi\, K^+)} = 0.908 \pm 0.194 \pm 0.100 \tag{12}$$

$$\frac{\mathcal{B}(B^+ \to \psi(2S)\, K^+)}{\mathcal{B}(B^0 \to J/\psi\, K^*(892)^0)} = 0.317 \pm 0.049 \pm 0.036$$

$$\frac{\mathcal{B}(B^0 \to \psi(2S)\, K^*(892)^0)}{\mathcal{B}(B^0 \to J/\psi\, K^*(892)^0)} = 0.515 \pm 0.113 \pm 0.052$$

$$\frac{\mathcal{B}(B^0 \to \psi(2S)\, K^*(892)^0)}{\mathcal{B}(B^+ \to \psi(2S)\, K^+)} = 1.62 \pm 0.41 \pm 0.19.$$

These ratios have been compared to two phenomenological calculations that use the factorization hypothesis. The calculations reproduce the overall features of the trends observed in the data.

We have also used the world-average [13] branching fraction $\mathcal{B}(B^+ \to J/\psi\, K^+)$ to determine the absolute branching fractions

$$\begin{aligned} \mathcal{B}(B^+ \to \psi(2S)\, K^+) &= (0.56 \pm 0.08 \pm 0.10) \times 10^{-3} \\ \mathcal{B}(B^0 \to \psi(2S)\, K^*(892)^0) &= (0.92 \pm 0.20 \pm 0.16) \times 10^{-3} \\ \mathcal{B}(B^0 \to J/\psi\, K^*(892)^0) &= (1.78 \pm 0.14 \pm 0.29) \times 10^{-3}. \end{aligned} \tag{13}$$

These measurements represent a significant improvement in the knowledge of B-meson decay rates into $\psi(2S)$ final states and contribute to an effective test of contemporary B-meson decay models.

VIII. ACKNOWLEDGMENTS

We thank the Fermilab staff and the technical staff at the participating institutions for their essential contributions to this research. This work was supported by the U. S. Department of Energy and National Science Foundation; the Natural Sciences and Engineering Research Council of Canada; the Istituto Nazionale di Fisica Nucleare of Italy; the Ministry of Education, Science, and Culture of Japan; the National Science Council of the Republic of China; the A. P. Sloan Foundation; the Swiss National Science Foundation; and the German Bundesministerium für Bildung, Wissenschaft, Forschung, und Technologie.

REFERENCES

[1] M. Wirbel, B. Stech, and M. Bauer, Z. Phys. C **29**, 637 (1985).
[2] M. Bauer, B. Stech, and M. Wirbel, Z. Phys. C **34**, 103 (1987).
[3] T. E. Browder, K. Honscheid, and D. Pedrini, Annu. Rev. Nucl. Part. Sci. **46**, 395 (1996).
[4] F. Abe *et al.* (CDF Collaboration), Phys. Rev. Lett. **75**, 1451 (1995).
[5] F. Abe *et al.* (CDF Collaboration), Phys. Rev. D **53**, 3496 (1996).
[6] F. Abe *et al.* (CDF Collaboration), Phys. Rev. D **57**, 5382 (1998).
[7] F. Abe *et al.* (CDF Collaboration), Phys. Rev. Lett. **75**, 3068 (1995).
[8] F. Abe *et al.* (CDF Collaboration), Phys. Rev. D **54**, 6596 (1996); Phys. Rev. Lett. **76**, 2015 (1996).
[9] M. Gourdin, A. N. Kamal, and X. Y. Pham, Phys. Rev. Lett. **73**, 3355 (1994); R. Aleksan, A. Le Yaouanc, L. Oliver, O. Pène, and J.-C. Raynal, Phys. Rev. D **51**, 6235 (1995).
[10] A. N. Kamal and A. B. Santra, Phys. Rev. D **51**, 1415 (1995); Z. Phys. C **72**, 91 (1996).
[11] F. Abe *et al.* (CDF Collaboration), Nucl. Instrum. Methods Phys. Res. A **271**, 387 (1988); D. Amidei *et al.*, Nucl. Instrum. Methods Phys. Res. A **350**, 73 (1994); F. Abe *et al.* (CDF Collaboration), Phys. Rev. D **52**, 4784 (1995); P. Azzi *et al.*, Nucl. Instrum. Methods Phys. Res. A **360**, 137 (1995).
[12] G. W. Foster, J. Freeman, C. Newman-Holmes, and J. Patrick, Nucl. Instrum. Methods Phys. Res. A **269**, 93 (1988).
[13] R. M. Barnett *et al.* (Particle Data Group), Phys. Rev. D **54**, 1 (1996) and 1997 off-year partial update for the 1998 edition (URL http://pdg.lbl.gov).
[14] G. S. Abrams *et al.* (Mark I Collaboration), Phys. Rev. Lett. **34**, 1181 (1975).
[15] T. A. Armstrong *et al.* (Fermilab E760 Collaboration), Phys. Rev. D **55**, 1153 (1997).
[16] J. Schwinger, K. A. Milton, W.-Y. Tsai, and L. L. DeRaad Jr., Proc. Natl. Acad. Sci. USA **72**, 4216 (1975); L. S. Brown and R. N. Cahn, Phys. Rev. Lett. **35**, 1 (1975); R. N. Cahn, Phys. Rev. D **12**, 3559 (1975).
[17] T. N. Pham, B. Pire, and T. N. Truong, Phys. Lett. **61B**, 183 (1976).
[18] C. Peterson, D. Schlatter, I. Schmitt, and P. M. Zerwas, Phys. Rev. D **27**, 105 (1983).
[19] P. Nason, S. Dawson, and R. K. Ellis, Nucl. Phys. **B327**, 49 (1989).
[20] A. D. Martin, W. J. Stirling, and R. G. Roberts, Phys. Rev. D **47**, 867 (1993).
[21] J. Chrin, Z. Phys. C **36**, 163 (1987).
[22] D. Coffman *et al.* (Mark III Collaboration), Phys. Rev. Lett. **68**, 282 (1992); **69**, 3689(E) (1992).
[23] A. Warburton, Ph.D. thesis, University of Toronto, 1998 (URL http://fnalpubs.fnal.gov/archive/1997/thesis/t-warburton.ps).
[24] M. Neubert, V. Rieckert, B. Stech, and Q. P. Xu, in *Heavy Flavours*, edited by A. J. Buras and M. Lindner (World Scientific, Singapore, 1992), p. 286.
[25] A. Deandrea, N. Di Bartolomeo, R. Gatto, and G. Nardulli, Phys. Lett. B **318**, 549 (1993); R. Casalbuoni *et al.*, Phys. Lett. B **299**, 139 (1993).
[26] H. Albrecht *et al.* (ARGUS Collaboration), Z. Phys. C **48**, 543 (1990).
[27] D. Bortoletto *et al.* (CLEO Collaboration), Phys. Rev. D **45**, 21 (1992).
[28] M. S. Alam *et al.* (CLEO II Collaboration), Phys. Rev. D **50**, 43 (1994).
[29] C. P. Jessop *et al.* (CLEO II Collaboration), Phys. Rev. Lett. **79**, 4533 (1997).

FIGURES

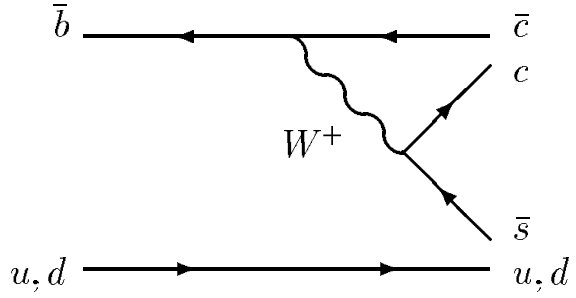

FIG. 1. Diagram of the color-suppressed internal-W emission mechanism for a B meson (here either a $\bar{b}u$ (B^+) or $\bar{b}d$ (B^0) state) decaying to charmonium (J/ψ or $\psi(2S)$) and a strange meson (K^+ or $K^*(892)^0$). In this process, the u or d quark is assumed to be a "spectator" of the weak interaction.

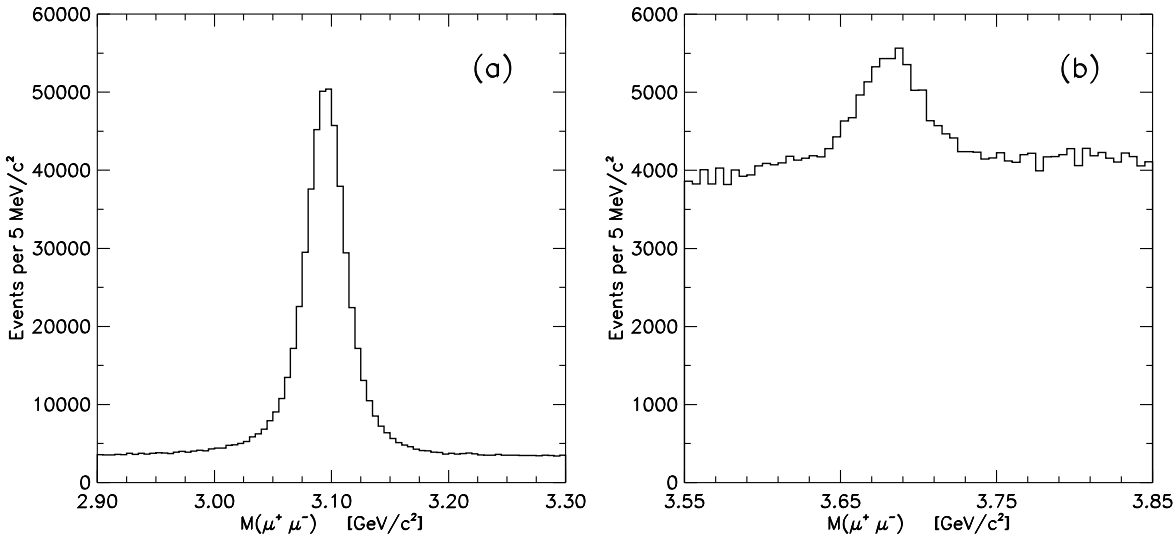

FIG. 2. The dimuon mass distributions for the inclusive J/ψ and $\psi(2S)$ candidate event samples are shown in (a) and (b), respectively.

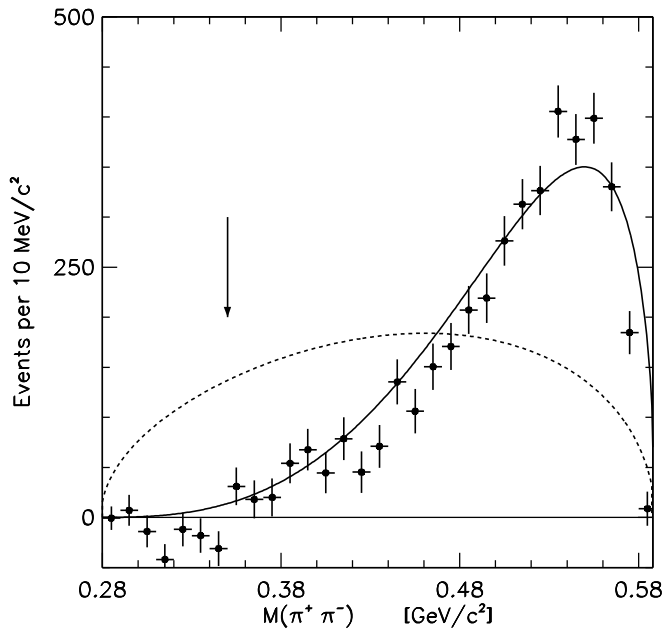

FIG. 3. The observed background-subtracted distribution of the dipion mass (points) in decays of the form $\psi(2S) \to J/\psi\,\pi^+\pi^-$. The arrow indicates the minimum mass required in the analysis. The solid curve represents a phenomenological prediction due to Pham *et al.* [17] and the broken curve describes a pure phase-space distribution.

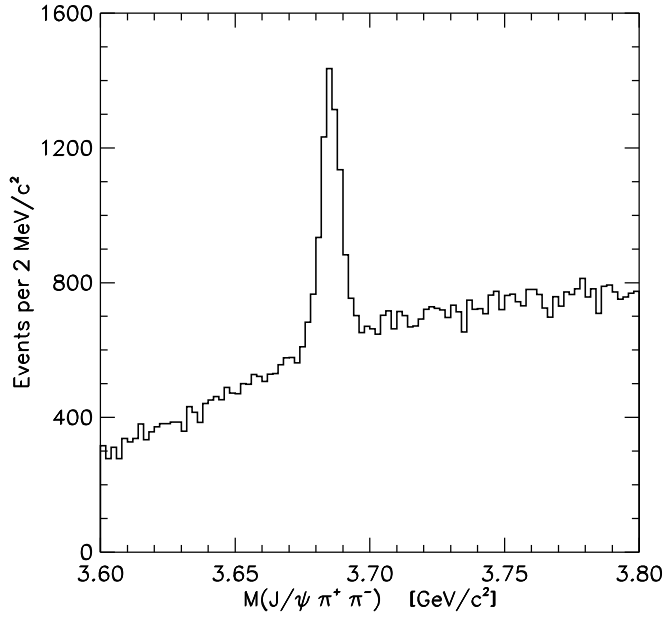

FIG. 4. The $J/\psi\,\pi^+\pi^-$ mass distribution for the $\psi(2S)$ candidates.

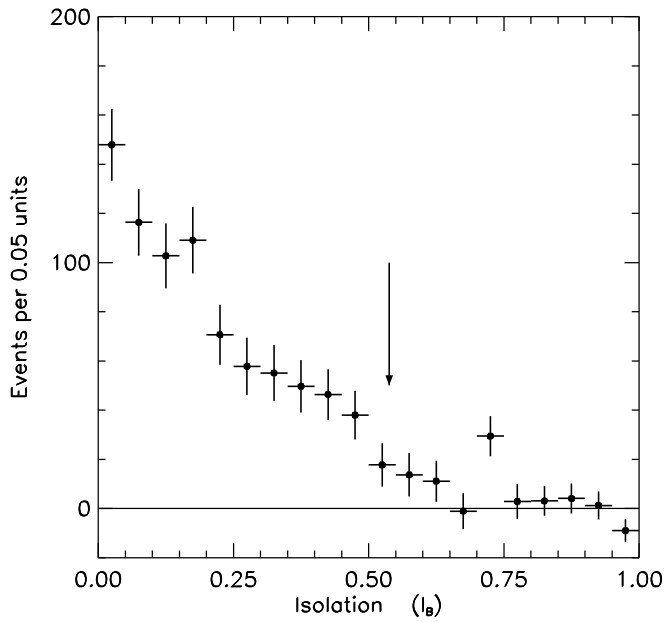

FIG. 5. The distribution of the isolation variable I_B for candidate $B^+ \to J/\psi K^+$ decays. A background subtraction has been performed using the sidebands in the $J/\psi K^+$ mass distribution. The arrow represents the cut below which candidates were accepted.

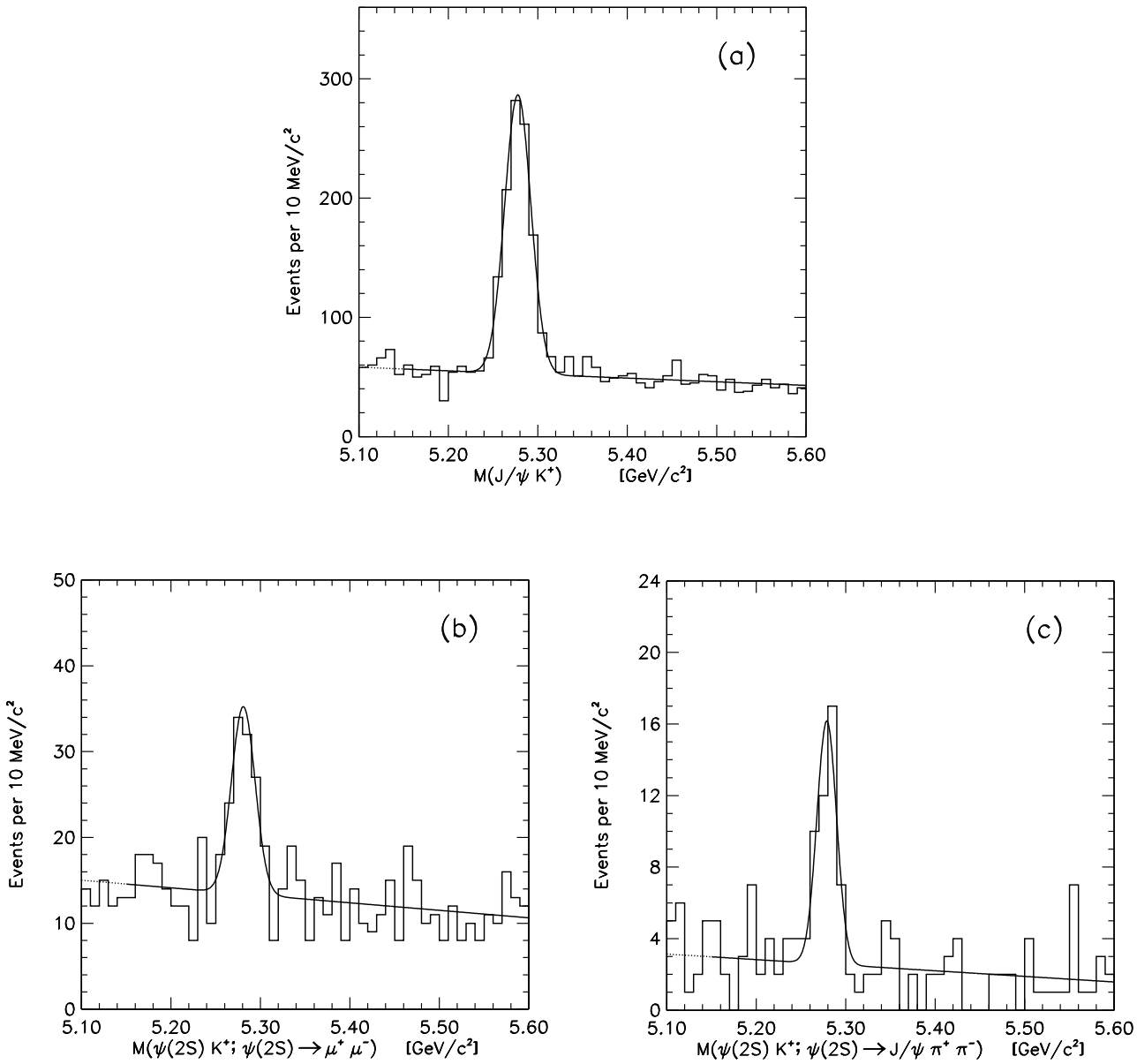

FIG. 6. The $J/\psi\, K^+$ mass distribution is shown in (a). The $\psi(2S)\, K^+$ mass distributions for the two modes $\psi(2S) \to \mu^+\mu^-$ and $\psi(2S) \to J/\psi\, \pi^+\pi^-$ are shown in (b) and (c), respectively. The curves are the results of a fit described in the text.

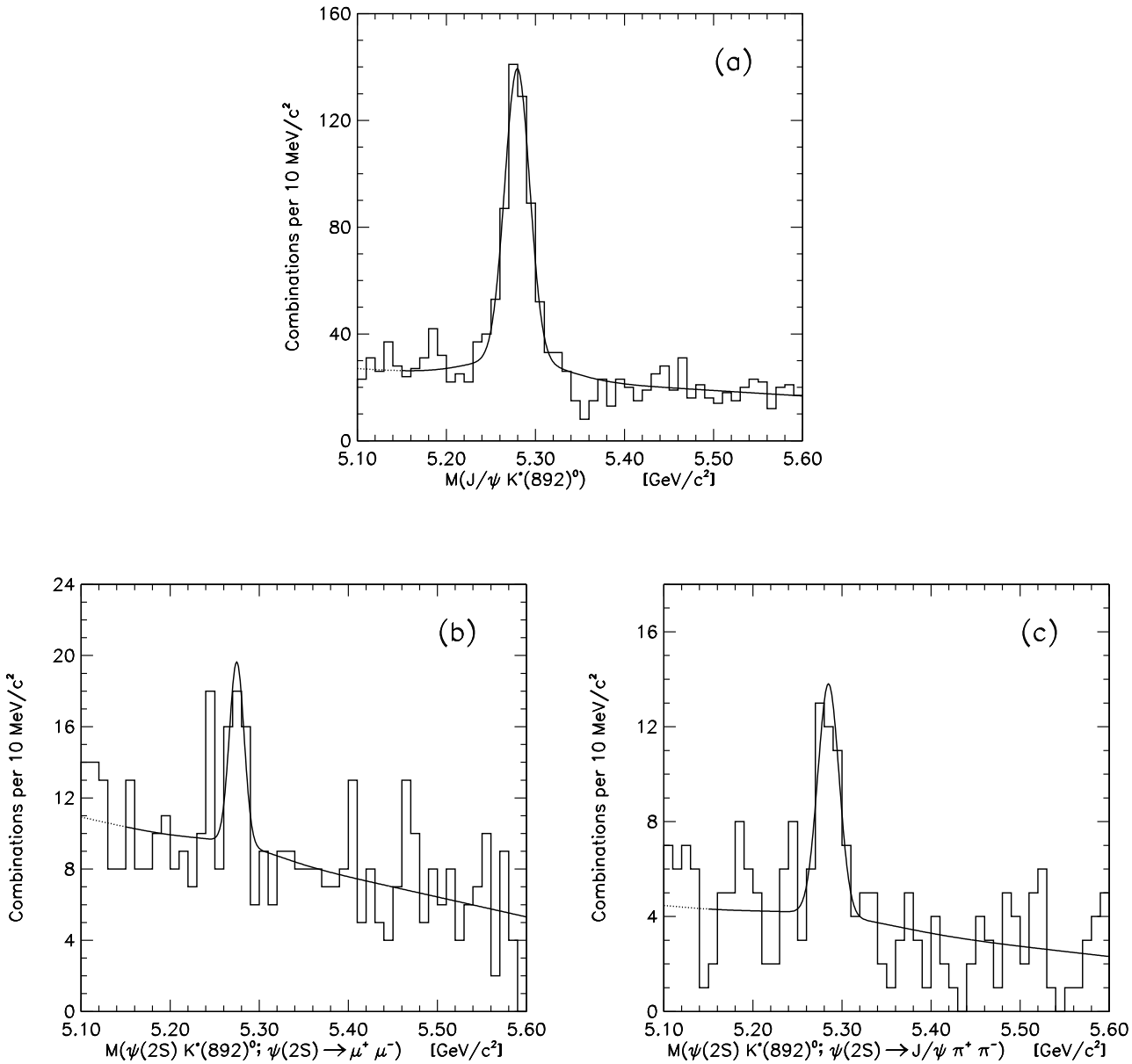

FIG. 7. The $J/\psi\, K^*(892)^0$ mass distribution is shown in (a). The $\psi(2S)\, K^*(892)^0$ mass distributions for the two modes $\psi(2S) \to \mu^+\mu^-$ and $\psi(2S) \to J/\psi\pi^+\pi^-$ are shown in (b) and (c), respectively. The curves are the results of a fit described in the text.

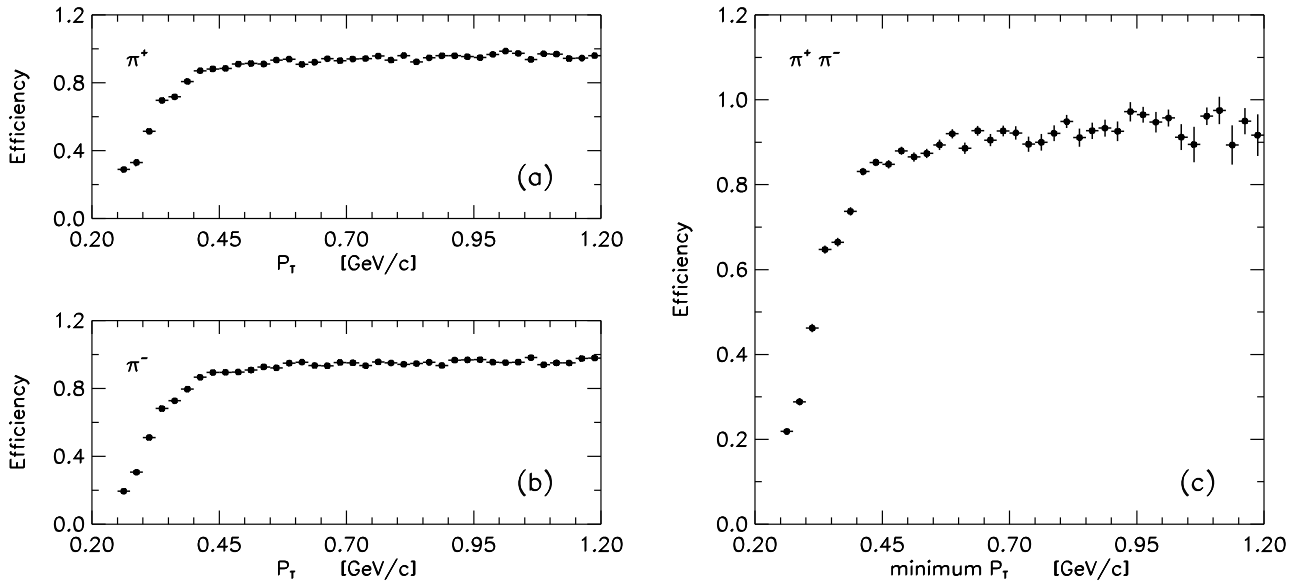

FIG. 8. The track reconstruction efficiency for π^+ mesons and π^- mesons as a function of the meson P_T is shown in (a) and (b), respectively. The dipion track reconstruction efficiency as a function of the lower momentum of the two pions is shown in (c).

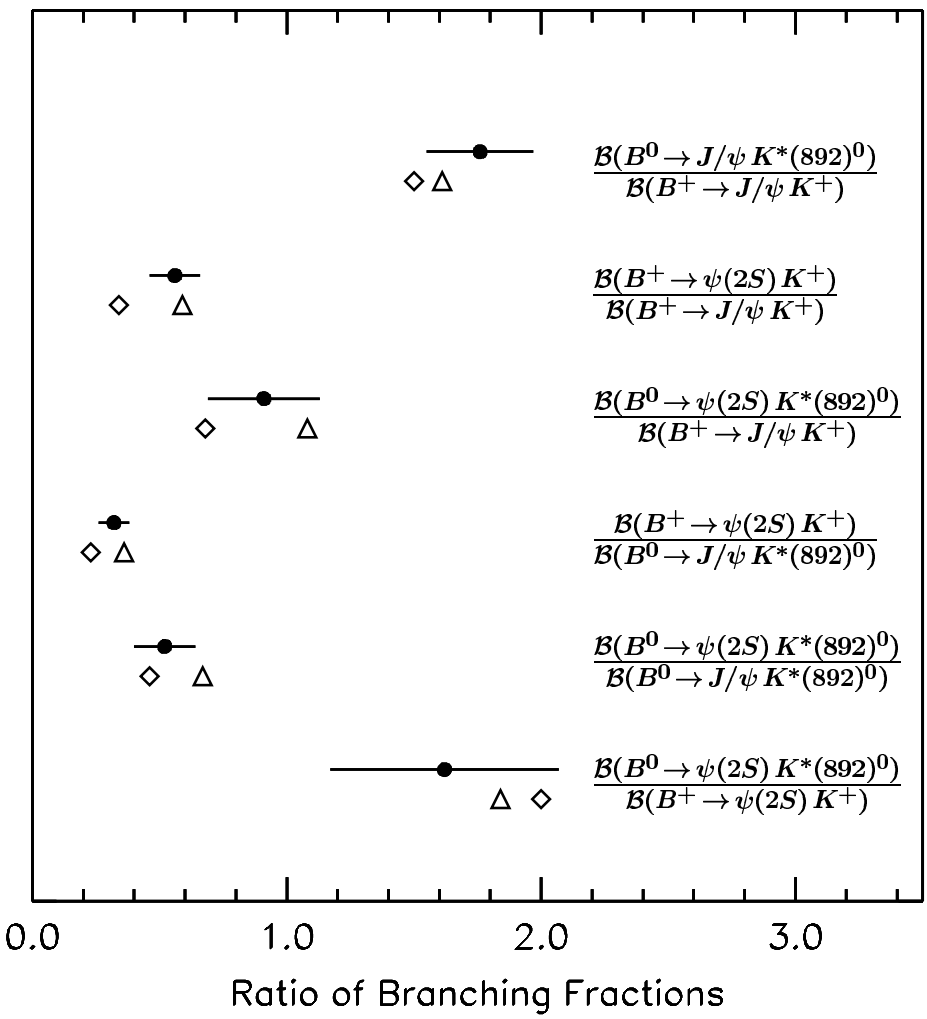

FIG. 9. Comparison of the measured branching-fraction ratios (filled circles) with theoretical predictions by Neubert *et al.* [24] (triangles) and Deandrea *et al.* [25] (diamonds). The error bars on the measured values represent the statistical and systematic uncertainties added in quadrature. In ratios involving B^+ and B^0 mesons, $f_u = f_d$ has been assumed.

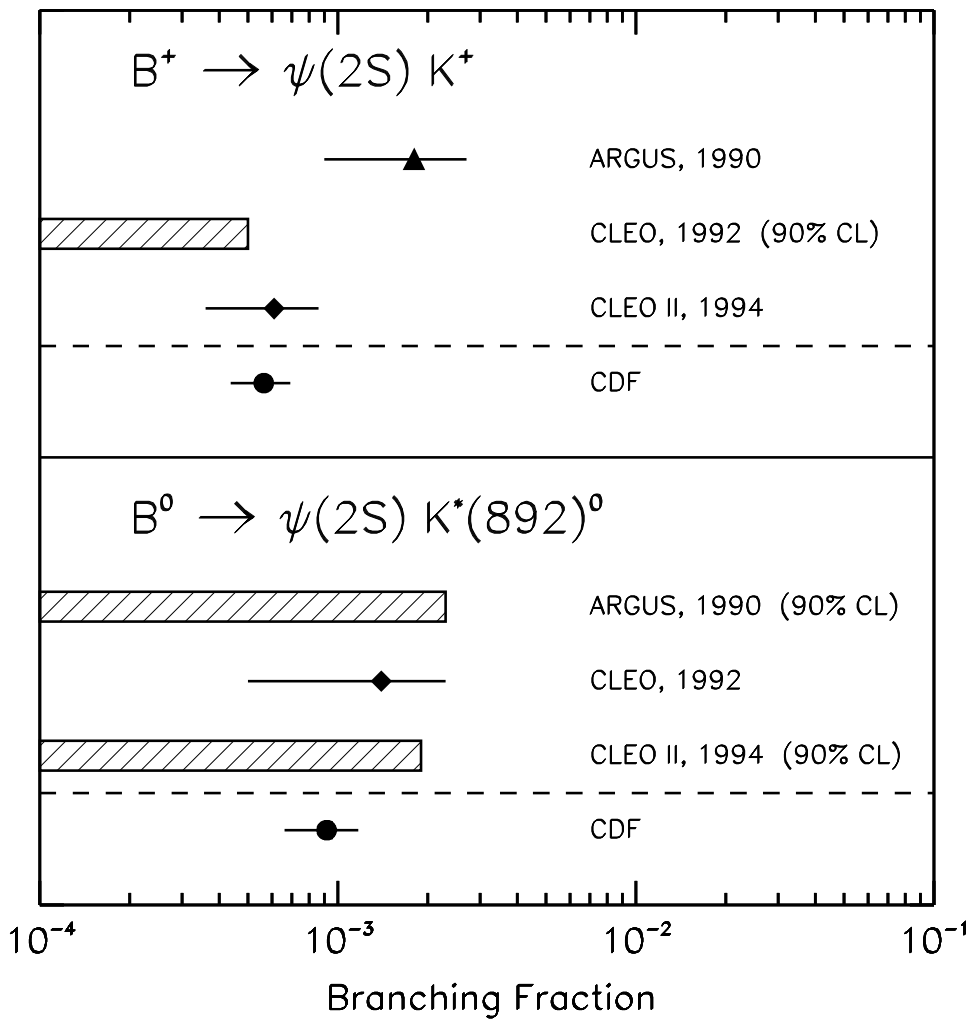

FIG. 10. A comparison of the derived CDF $\mathcal{B}(B^+ \to \psi(2S)\,K^+)$ and $\mathcal{B}(B^0 \to \psi(2S)\,K^*(892)^0)$ absolute branching fractions with measurements and limits from the ARGUS [26], CLEO [27], and CLEO II [28] experiments. The hatched bars denote 90% confidence-level (C.L.) upper limits and the error bars represent the statistical, systematic, and branching-fraction uncertainties added in quadrature.

TABLES

TABLE I. The ratios of the peak amplitudes and widths of the Gaussian parametrizations describing the wrong to right K-π mass assignments in the $K^*(892)^0$ reconstruction.

B-Meson Decay	$c\bar{c}$ Mode	Amplitude Ratio	Width Ratio
$B^0 \to J/\psi\, K^*(892)^0$	$J/\psi \to \mu^+\mu^-$	0.068	3.6
$B^0 \to \psi(2S)\, K^*(892)^0$	$\psi(2S) \to \mu^+\mu^-$	0.046	5.8
$B^0 \to \psi(2S)\, K^*(892)^0$	$\psi(2S) \to J/\psi\,\pi^+\pi^-$	0.043	6.3

TABLE II. The numbers of observed signal events, the fitted masses, and the signal widths for the six different B-decay reconstructions. The listed uncertainties are statistical only.

B-Meson Decay	$c\bar{c}$ Mode	Event Yield	Mass [MeV/c^2]	Width [MeV/c^2]
$B^+ \to J/\psi\, K^+$	$J/\psi \to \mu^+\mu^-$	856.7 ± 38.3	5278 ± 1	14.6 ± 0.6
$B^+ \to \psi(2S)\, K^+$	$\psi(2S) \to \mu^+\mu^-$	71.9 ± 13.4	5281 ± 3	13.1 ± 2.2
$B^+ \to \psi(2S)\, K^+$	$\psi(2S) \to J/\psi\,\pi^+\pi^-$	37.4 ± 7.4	5279 ± 2	11.0 ± 2.0
$B^0 \to J/\psi\, K^*(892)^0$	$J/\psi \to \mu^+\mu^-$	378.8 ± 24.8	5280 ± 1	13.9 ± 1.1
$B^0 \to \psi(2S)\, K^*(892)^0$	$\psi(2S) \to \mu^+\mu^-$	20.9 ± 7.3	5275 ± 3	8.2 ± 2.4
$B^0 \to \psi(2S)\, K^*(892)^0$	$\psi(2S) \to J/\psi\,\pi^+\pi^-$	29.1 ± 7.5	5285 ± 4	11.9 ± 3.3

TABLE III. A summary of the absolute products of the geometric and kinematic acceptances, calculated for each decay mode for B mesons produced with $k_T > 5.0$ GeV/c and $|y_b| < 1.1$. The uncertainties given are due to Monte Carlo statistics alone.

B-Meson Decay	$c\bar{c}$ Mode	Acceptance ($\times 10^{-3}$)
$B^+ \to J/\psi\, K^+$	$J/\psi \to \mu^+\mu^-$	19.2 ± 0.3
$B^+ \to \psi(2S)\, K^+$	$\psi(2S) \to \mu^+\mu^-$	21.8 ± 0.3
$B^+ \to \psi(2S)\, K^+$	$\psi(2S) \to J/\psi\,\pi^+\pi^-$	6.3 ± 0.2
$B^0 \to J/\psi\, K^*(892)^0$	$J/\psi \to \mu^+\mu^-$	7.8 ± 0.2
$B^0 \to \psi(2S)\, K^*(892)^0$	$\psi(2S) \to \mu^+\mu^-$	8.3 ± 0.2
$B^0 \to \psi(2S)\, K^*(892)^0$	$\psi(2S) \to J/\psi\,\pi^+\pi^-$	3.9 ± 0.1

TABLE IV. A summary of the geometric and kinematic acceptance ratios with associated systematic uncertainties, combined in quadrature, from the following sources: Monte Carlo statistics, the generated B-meson P_T spectrum, trigger effects, helicity effects, and the CDF detector simulation uncertainty.

Numerator \ Denominator	$B^+ \to J/\psi\, K^+$ $\hookrightarrow \mu^+\,\mu^-$	$B^0 \to J/\psi\, K^*(892)^0$ $\hookrightarrow \mu^+\,\mu^-$	$B^+ \to \psi(2S)\, K^+$ $\hookrightarrow \mu^+\,\mu^-$
$B^0 \to J/\psi\, K^*(892)^0$ $\hookrightarrow \mu^+\,\mu^-$	0.405 ± 0.025		
$B^+ \to \psi(2S)\, K^+$ $\hookrightarrow \mu^+\,\mu^-$	1.137 ± 0.084	2.810 ± 0.285	
$B^+ \to \psi(2S)\, K^+$ $\hookrightarrow J/\psi\,\pi^+\,\pi^-$	0.329 ± 0.017	0.813 ± 0.058	0.289 ± 0.026
$B^0 \to \psi(2S)\, K^*(892)^0$ $\hookrightarrow \mu^+\,\mu^-$	0.431 ± 0.044	1.066 ± 0.092	0.379 ± 0.030
$B^0 \to \psi(2S)\, K^*(892)^0$ $\hookrightarrow J/\psi\,\pi^+\,\pi^-$	0.201 ± 0.017	0.496 ± 0.032	0.177 ± 0.023

TABLE V. A summary of the efficiency-product ratios and their associated systematic uncertainties from the following sources: track reconstruction efficiencies, confidence-level criteria efficiencies, and decay-length requirement efficiencies.

Numerator \ Denominator	$B^+ \to J/\psi\, K^+$ $\hookrightarrow \mu^+\mu^-$	$B^0 \to J/\psi\, K^*(892)^0$ $\hookrightarrow \mu^+\mu^-$	$B^+ \to \psi(2S)\, K^+$ $\hookrightarrow \mu^+\mu^-$
$B^0 \to J/\psi\, K^*(892)^0$ $\hookrightarrow \mu^+\mu^-$	0.930 ± 0.030		
$B^+ \to \psi(2S)\, K^+$ $\hookrightarrow \mu^+\mu^-$	0.980 ± 0.023	1.05 ± 0.03	
$B^+ \to \psi(2S)\, K^+$ $\hookrightarrow J/\psi\, \pi^+\pi^-$	0.703 ± 0.055	0.755 ± 0.062	0.717 ± 0.056
$B^0 \to \psi(2S)\, K^*(892)^0$ $\hookrightarrow \mu^+\mu^-$	0.923 ± 0.030	0.992 ± 0.024	0.942 ± 0.031
$B^0 \to \psi(2S)\, K^*(892)^0$ $\hookrightarrow J/\psi\, \pi^+\pi^-$	0.651 ± 0.053	0.700 ± 0.055	0.664 ± 0.054

TABLE VI. Branching fractions of the daughter-meson decay modes reconstructed in the present analysis. The world-average branching fractions were used for the charmonium mesons [13]. Note that the branching fraction for the $\psi(2S) \to \mu^+\mu^-$ decay assumes lepton universality. The $K^*(892)^0$ branching fraction is based on isospin symmetry.

Decay Mode	Branching Fraction
$J/\psi \to \mu^+\mu^-$	$(6.01 \pm 0.19) \times 10^{-2}$
$\psi(2S) \to \mu^+\mu^-$	$(8.5 \pm 0.7) \times 10^{-3}$
$\psi(2S) \to J/\psi\, \pi^+\pi^-$	$(3.07 \pm 0.19) \times 10^{-1}$
$K^*(892)^0 \to K^+\pi^-$	$2/3$

TABLE VII. The measured ratios of branching fractions times fragmentation fractions for the four decay modes. The systematic uncertainties have been calculated taking into account cancellations and correlations in uncertainties.

Quantity	Measured Ratio
$\frac{f_d}{f_u} \cdot \frac{\mathcal{B}(B^0 \to J/\psi K^*(892)^0)}{\mathcal{B}(B^+ \to J/\psi K^+)}$	$1.76 \pm 0.14 \pm 0.15$
$\frac{\mathcal{B}(B^+ \to \psi(2S) K^+)}{\mathcal{B}(B^+ \to J/\psi K^+)}$	$0.558 \pm 0.082 \pm 0.056$
$\frac{f_d}{f_u} \cdot \frac{\mathcal{B}(B^0 \to \psi(2S) K^*(892)^0)}{\mathcal{B}(B^+ \to J/\psi K^+)}$	$0.908 \pm 0.194 \pm 0.100$
$\frac{f_u}{f_d} \cdot \frac{\mathcal{B}(B^+ \to \psi(2S) K^+)}{\mathcal{B}(B^0 \to J/\psi K^*(892)^0)}$	$0.317 \pm 0.049 \pm 0.036$
$\frac{\mathcal{B}(B^0 \to \psi(2S) K^*(892)^0)}{\mathcal{B}(B^0 \to J/\psi K^*(892)^0)}$	$0.515 \pm 0.113 \pm 0.052$
$\frac{f_d}{f_u} \cdot \frac{\mathcal{B}(B^0 \to \psi(2S) K^*(892)^0)}{\mathcal{B}(B^+ \to \psi(2S) K^+)}$	$1.62 \pm 0.41 \pm 0.19$